Hydrodynamic Heat Transport in Compact and Holey Silicon Thin Films

A. Beardo,[1,*] M. Calvo-Schwarzwälder,[2,3] J. Camacho,[1] T.G. Myers,[3] P. Torres,[1] L. Sendra,[1] F.X. Alvarez,[1] and J. Bafaluy[1]

[1] *Physics Department, Universitat Autònoma de Barcelona, 08193 Bellaterra, Spain*
[2] *Mathematics Department, Universitat Politècnica de Catalunya, 08028 Barcelona, Spain*
[3] *Centre de Recerca Matemàtica, Campus de Bellaterra, Edifici C, 08913 Barcelona, Spain*

(Received 16 October 2018; revised manuscript received 1 December 2018; published 1 March 2019)

A multiscale hydrodynamic-heat-transport model applicable to arbitrary geometries using finite-element methods is compared with the experimental effective thermal conductivity of silicon thin films and periodic holey membranes for different sizes and temperatures. The range of system length scales and temperatures in which the model predictions agree with experimental data is discussed and quantitatively determined. The model agrees with experimental results when the smallest system size is larger than twice the nonlocal length, an intrinsic property of the material that depends only on temperature. These results open the door to the use of the hydrodynamic equation instead of an effective Fourier model to interpret current heat-transport experimental data.

DOI: 10.1103/PhysRevApplied.11.034003

I. INTRODUCTION

One of the most-important limitations in electronic engineering is related to heat management [1]. The reduction of the characteristic length scales of electronic devices has led to two important problems: on one hand, scale reduction has reduced the capacity of these components to release their excess heat into the substrate [2–4]; on the other hand, device miniaturization has multiplied the number of components per unit area, thus increasing the heat generated [1]. Both effects lead to the generation of hot spots that limit the computational speed of the devices and are a potential source of damage. Thus the proper management of heat transport at small scales is necessary to improve the performance of electronic devices. The difficulties arise because at small scales geometric effects reduce thermal conduction in a way that is currently not well understood. For example, recent experimental results in semiconductors have been shown not to obey Fourier's law [2–4].

When one is studying heat transport in semiconductors the usual starting point is the Boltzmann transport equation (BTE) [5–7]. This equation relates the time and space derivatives of the phonon distribution function to the phonon collisions that restore the equilibrium. The complexities of the collision term make solving the BTE a difficult task even in the linearized case. As a result, the modeling of thermal transport in nanostructures has often been based on the relaxation-time approximation [8,9]. One important drawback of this approach is that it does not properly account for the effects of normal, momentum-conserving, collisions, which are treated as resistive. In recent years, new numerical methods have been developed that overcome this shortcoming by taking into account the details of the linearized collision term [10–12]. These have been successfully applied to bulk crystals, but the inclusion of size effects in these approaches is still a challenge that limits their practical use to simple geometries [13–15].

Alternative approaches have been proposed with the aim of obtaining the maximum predictability with the minimum complexity in the transport equations [16–18]. One of these approaches, the kinetic collective model (KCM) [17,19], relates most of the non-Fourier behavior of heat transport to the appearance of nonlocal and memory effects. By linearizing the BTE and taking into account the effect of the momentum- and energy-conservation laws in the collision operator, one obtains a generalized heat-transport equation. The final form is similar to the Navier-Stokes equation (NSE) for fluids. The KCM predicts diffusive transport when the system size is much larger than phonon mean free paths (MFPs) and predicts hydrodynamic behavior when a system dimension becomes comparable to the MFPs. The hydrodynamic heat equation is simple enough to be implemented with finite elements and, consequently, can be used in arbitrary complex geometries. The parameters appearing in the equation are intrinsic properties of the material (they do not depend on the system geometry) and can be obtained from microscopic calculations [19,20]. Geometry effects are captured through the appropriate boundary conditions, so the model

*albert.beardo@uab.cat

can predict the thermal response of systems of arbitrary geometry. Recently, it was successfully applied to the results of heater-line and grating experiments displaying non-Fourier behavior [2,20].

The main difficulty of this approach is that the MFP of the phonons can span several orders of magnitude [21–23]. As the characteristic size of the devices is reduced, boundary effects become more important. In the first stages of the appearance of boundary effects, most of the phonons have a MFP shorter than the size of the sample, and the effects on the heat flux will be noticed only in a region near the boundary. As the system becomes smaller, ballistic effects are apparent for an increasing number of phonon modes [22,23]. Since the KCM summarizes the whole MFP spectrum as an average quantity, the nonlocal length, one may expect the model to be oversimplified for sufficiently small system sizes, where heat transport becomes mostly ballistic.

The goal of this work is twofold: (i) to show the applicability of the KCM to different geometries by comparing theoretical and experimental results (here we focus specifically on compact thin films and periodic holey films); (ii) to explore the range of system sizes and temperatures where model predictions match experimental results.

The paper is organized as follows: In Sec. II, we introduce the hydrodynamic-heat-transport equation with averaged coefficients obtained from *ab initio* calculations. In Sec. III, we discuss the applicability of the model in silicon samples by comparing the numerical solution of the hydrodynamic-heat-transport equation with experimental data in thin films. From this study a criterion for the applicability of the model is proposed. In Sec. IV, we show the usefulness of the approach by comparing the model with experimental data for a holey membrane, and verify the applicability criterion found in the previous section. Finally, Sec. IV is devoted to concluding remarks.

II. KINETIC COLLECTIVE MODEL

The solution of the linearized BTE proposed by Guyer and Krumhansl [5] is based on the splitting of the collision operator C into normal N and resistive R components such that $C = N + R$. The basis used is the one that diagonalizes the operator N. In the isotropic dispersionless approximation, the corresponding eigenvectors can be identified with the different order perturbations of the phonon distribution function. The use of this approach is based on the different effects that the two scattering mechanisms have on the different moments of the distribution. Energy density (the zero-order moment) is unaffected by both normal and resistive collisions. The heat flux $\mathbf{q}$ (related to the first moment) can be relaxed by resistive scattering but not by normal scattering. Finally, both normal and resistive collisions can relax higher-order moments. Here we propose that most of the out-of-equilibrium behavior in thermal transport can be derived from this distinction. Other phenomena related to the different existent resistive collisions are only second-order corrections. In the original work by Guyer and Krumhansl [5], nonlocal effects and memory effects were explicitly obtained in the collective regime, where normal scattering is dominant. The resulting equations are the energy-conservation equation and the hydrodynamic-heat-transport equation respectively:

$$c\frac{dT}{dt} + \nabla \cdot \mathbf{q} = 0, \tag{1}$$

$$\tau\frac{\partial \mathbf{q}}{\partial t} + \mathbf{q} + \kappa\nabla T = \ell^2(\nabla^2\mathbf{q} + 2\nabla\nabla \cdot \mathbf{q}), \tag{2}$$

where c is the specific heat, κ is the bulk thermal conductivity, τ is the heat-flux relaxation time, and ℓ is the nonlocal characteristic length. These parameters are intrinsic properties of the material (i.e., independent of the geometry).

Nonlocal effects in the heat flux are also present in the kinetic regime, where resistive scattering is dominant. In recent work [7], an explicit derivation for this regime was obtained by a perturbation expansion of the BTE around the nonequilibrium distribution obtained by the maximum-entropy principle. Equation (2) was obtained, with slight differences in the coefficients on the right-hand side, which indicates that the underlying mechanisms leading to nonlocal effects are not equivalent in the different regimes. Since in this work we consider stationary situations ($\nabla \cdot \mathbf{q} = 0$ and $\partial\mathbf{q}/\partial t = 0$), the only difference between the kinetic and the collective transport equation is the microscopic expressions of the bulk thermal conductivity κ and the nonlocal length ℓ.

In most situations, such as with silicon at not extremely low temperatures, normal and resistive collisions occur, and the nonlocal and memory effects associated with both mechanisms should be taken into account [19]. The KCM proposes an effective hydrodynamic-heat-transport equation of the form of Eq. (2) by averaging the hydrodynamic parameters in the kinetic and collective situations. The use of the hydrodynamic equation is not restricted to the usual hydrodynamic regime, where normal collisions are dominant. The KCM is a multiscale model that provides the required expressions for the thermal conductivity and the nonlocal length in terms of microscopic information such as phonon scattering rates and dispersion relations that are obtained from *ab initio* calculations. Explicit microscopic expressions for these parameters can be found in supplementary Sec. S2 in Ref. [20], and can be calculated with the open-source KCM code [24]. In particular, the nonlocal length ℓ is an average over normal- and resistive-collision MFPs. With this approach, one assumes that the nonlocal effects can be effectively captured by a single characteristic length ℓ. This description is adequate

if the system length scale is larger than a significant part of the MFP spectrum, but one expects it to fail for system sizes much smaller than ℓ, where ballistic scattering becomes important. As stated above, one of the aims of this work is to explore the range of validity of this treatment.

Equation (2) is analogous to the NSE, and hence phenomenological interpretation of heat-flux behavior may be inferred from known results of fluid dynamics. Specifically, the right-hand-side terms are analogous to the viscous terms of the NSE, and concepts such as friction and vorticity become relevant [20]. Furthermore, using an analogy with the flow of rarefied gases with large Knudsen number, one may use a slip boundary condition, with characteristic length of order ℓ, for the heat flux tangential to the boundary $\mathbf{q}_t$ [25]:

$$\mathbf{q}_t = -C\ell\, \nabla \mathbf{q}_t \cdot \mathbf{n}, \tag{3}$$

$$\mathbf{q} \cdot \mathbf{n} = 0, \tag{4}$$

where $\mathbf{n}$ is the outward-pointing normal and C is a dimensionless constant that can be defined in terms of the specularity of the surface. Diffusive phonon scattering in boundaries corresponds to $C = 1$ and purely specular phonon scattering corresponds to $C \to \infty$ [25]. The value of C depends on temperature and can be determined by comparison between the wavelength of the phonons and the average height of the roughness defects η [26,27]:

$$C = \frac{1+p}{1-p}, \tag{5}$$

where p is the specularity defined as

$$p = \frac{\sum_{\mathbf{k}} c_{\mathbf{k}} e^{-\pi(4\pi\eta\cos\theta/\lambda_{\mathbf{k}})^2}}{\sum_{\mathbf{k}} c_{\mathbf{k}}}, \tag{6}$$

where $c_{\mathbf{k}}$ and $\lambda_{\mathbf{k}}$ are the specific heat and the wavelength of the phonon mode with wave vector $\mathbf{k}$, respectively, and θ is the angle of incidence obtained from the normal vector to the surface $\mathbf{n}$ and the wave vector with use of $\cos\theta = \mathbf{n}\cdot\mathbf{k}/|\mathbf{k}|$. As a reference, in silicon, values of C larger than 2 require roughness defects to be smaller than 0.2 nm.

Once the parameters τ, ℓ, κ, and C have been calculated, Eqs. (1) and (2), complemented with the boundary conditions (3) and (4), can be numerically solved in complex geometries through finite-element methods; see the Appendix for details on the Galerkin-method implementation of the equations using COMSOL MULTIPHYSICS. We next compare the hydrodynamic predictions with results from experiments on silicon samples for two geometries: compact thin films and holey thin films. In both cases we obtain the stationary temperature and heat-flux profiles when a temperature difference is imposed between the ends of the system, and discuss the range of system sizes and temperatures where model predictions match experimental results.

III. COMPACT THIN FILMS

The typical heat-flux profile obtained by the hydrodynamic model in a thin film is depicted in Fig. 1. It demonstrates the appearance of a boundary layer, with characteristic size 2ℓ, in which the heat flux is reduced due to the nonlocal effects originating from the boundaries; this size does not change appreciably for finite values of C (Fig. 1). For film widths much larger than ℓ, the effect is negligible in most of the cross section and the behavior is essentially the flat Fourier heat-flux profile. As the size decreases, the effect increases and it is responsible for the reduction of the effective thermal conductivity; namely,

$$\kappa_{\mathrm{ef}} = \frac{\int_\Gamma |\mathbf{q}| d\Gamma}{S\Delta T/L}, \tag{7}$$

where Γ is the cross section, S is its area, ΔT is the imposed temperature difference, and L is the distance between the ends of the system.

To validate the model in silicon samples and quantitatively identify the range of applicability of the model, we consider available experimental data for the effective thermal conductivity κ_{ef} of silicon thin films of different widths w and temperatures [26,28,29]. For high temperatures, diffusive boundary reflections ($C = 1$) can be assumed so as to predict the effective thermal conductivity of the samples considered. However, the authors of [26,28,29] estimate a small average roughness-defect height η in the samples, which has a significant effect on the effective thermal

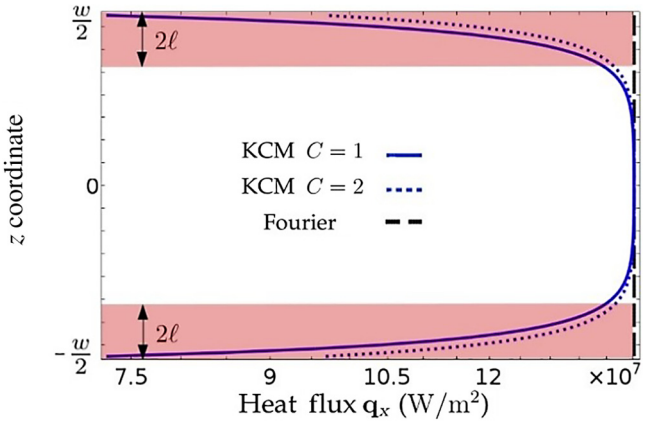

FIG. 1. Heat-flux profile for a silicon thin film of width $w = 3\ \mu$m at $T = 300$ K predicted by the Fourier model (dashed line) and the KCM for $C = 1$ (solid line) and $C = 2$ (dotted line). The reduction of $\mathbf{q}$ at the boundaries in the KCM has a nonlocal effect of characteristic size 2ℓ, which is the cause of the effective-thermal-conductivity reduction. We refer to this region (indicated in red) as the "boundary layer".

conductivity at lower temperatures. Hence, consistent with Refs. [26,28–30], here we assume $\eta = 0.3$ nm. Using Eqs. (5) and (6) over the range of temperatures used in the experiments, we obtain a constant specularity parameter $C = 1.5$ above 100 K.

Figure 2(a) shows the predictions for thin films of different widths w at room temperature. It is clear that the model predictions reproduce the experimental data for sufficiently large sizes. Specifically, one observes agreement for widths on the order more than 2ℓ ($\ell = 176$ nm for silicon at $T = 300$ K, with use of the expression for ℓ in Ref. [20]).

In Fig. 2(b), we consider the experimental data for three different thin-film widths at different temperatures. When the temperature is reduced, the characteristic nonlocal length ℓ increases because the phonon MFP increases. The model predictions agree with experimental data again when the geometry-limiting dimension w is larger than twice the nonlocal length ℓ. To further clarify this, in Fig. 2(c) the temperature dependence of ℓ is shown. Consistent with Figs. 2(a) and 2(b), the gray region identifies the temperatures and widths for which the hydrodynamic model is accurate.

Remarkably, we thus find that the condition $w > 2\ell$ provides a unifying criterion for the validity of the model for any size and temperature. This corresponds to the case where the top and bottom boundary layers do not completely overlap (see Fig. 1). In this situation most of the phonon modes do not behave ballistically and the hydrodynamic description through a single characteristic length ℓ is adequate. In the next section, we analyze if this criterion applies to a different geometry.

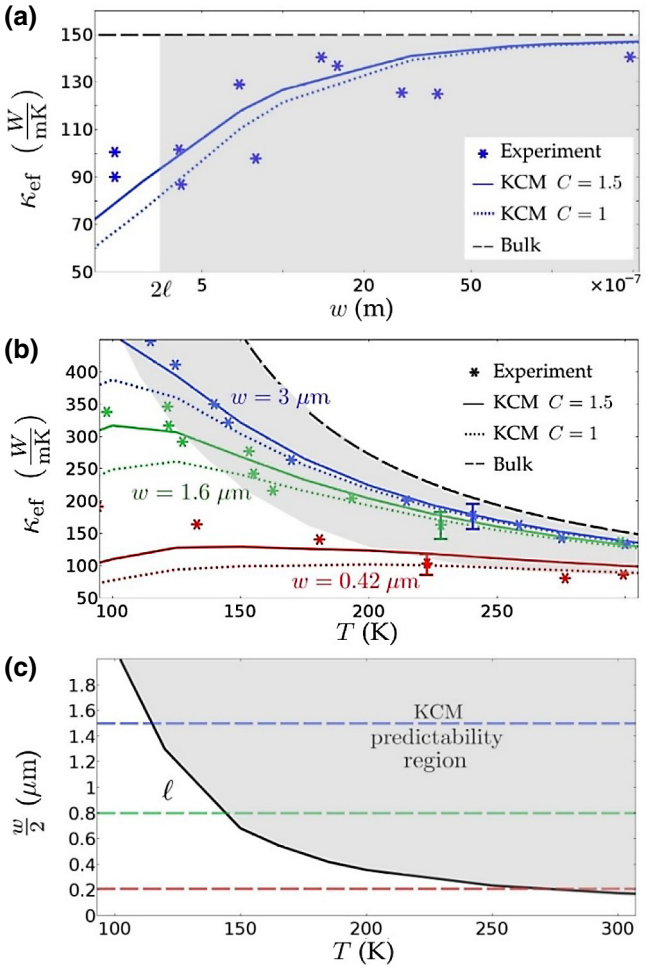

FIG. 2. Thin-film experimental [26,28,29] and predicted thermal conductivities versus (a) width at room temperature and (b) temperature for different widths. Two values of the C related to phonon scattering at the surface are shown: $C = 1$ (diffusive scattering, i.e., large roughness) and $C = 1.5$ ($\eta = 0.3$ nm). (c) Temperature dependence of the nonlocal length ℓ. The dashed colored lines refer to the thin films considered in (b). In (a)–(c) the KCM applicability region ($w > 2\ell$) is indicated in gray.

IV. HOLEY THIN FILMS

In this section we use the experimental data from Ref. [31] for periodic holey silicon membranes with different widths w, periodicity a, and pore diameters d at different temperatures (see Fig. 4). In this case, the temperature difference in the simulations is established in one periodic unit. Large roughness defects were reported in Ref. [31] (much larger than 0.3 nm) indicating $C = 1$ (i.e., diffusive boundary scattering). Moreover, surface damage from the fabrication process is expected in the curved surfaces of the pores. The authors of [31] indicate that an increase of 0.5 μm in the diameter could be assumed to account for this. With this consideration, two systems are studied: holey film A, with periodicity $a = 20$ μm, diameter $d = 11.4$ μm, and width $w = 4.84$ μm; and holey film B, with $a = 4$ μm, $d = 2.8$ μm, and $w = 4.49$ μm. In both cases the pores are aligned.

In Fig. 3 we compare the experimental effective conductivity with the KCM prediction and the Fourier prediction (which accounts only for the volume-reduction effect).

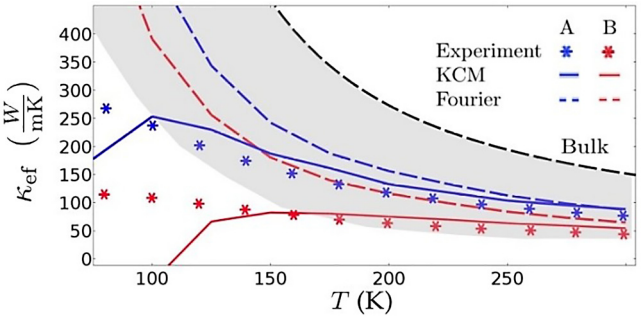

FIG. 3. Experimental thermal conductivities of periodic holey films [31] versus temperature compared with the KCM and Fourier predictions. The KCM applicability region is indicated in gray.

We find agreement between theory and experimental data except at low temperatures. To analyze if the validity criterion found in the previous section also applies to this system, Fig. 3 displays the region satisfying the criterion. For the larger holey film A the criterion is $w > 2\ell$ because the limiting dimension is the width, the same as with thin films. For the smaller holey film B the limiting dimension is the neck $a - d = 1.2\ \mu$m, so the expected range of applicability is $a - d > 2\ell$. Remarkably, one observes that the KCM correctly predicts the experimental data within the regions satisfying the criterion, and it starts to fail just outside, where it underestimates them.

To illustrate the effect of the temperature dependence on the boundary layer in Fig. 4 we compare the Fourier and the KCM heat-flux profiles along the line intersecting the center of two contiguous pores in holey film B. For sufficiently high temperatures, the regions affected by different boundary layers do not completely overlap (and hence the Fourier and the KCM predictions do not differ much in the central point between two pores).

Song and Chen [31] showed that the experimental measurement of the effective conductivity is unchanged by considering a staggered pattern for the pore positions with similar geometric dimensions. This is consistent with the fact that when the relative positions of the pores are changed, the KCM predictions differ by just a few percent. Moreover, the good agreement between the model and theory confirms that the effect of oxide layers in the surfaces is negligible at the length scales considered.

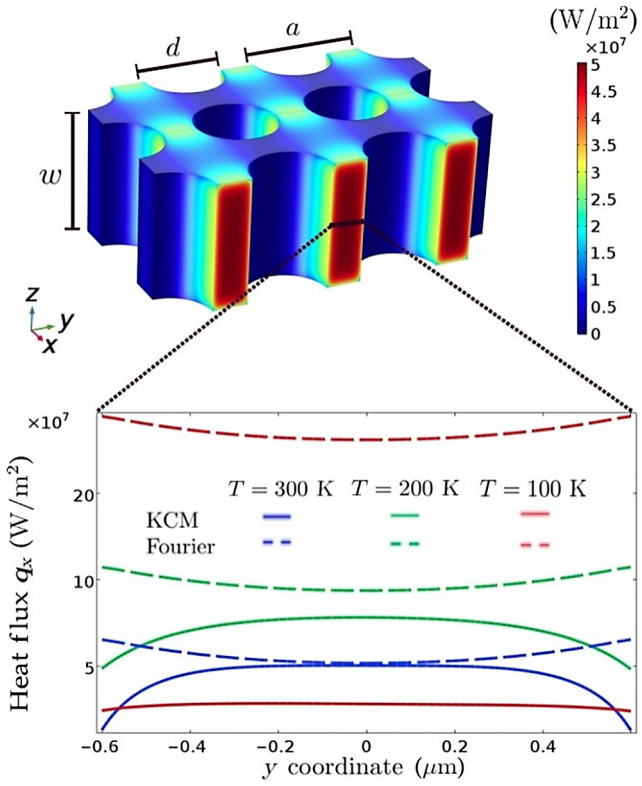

FIG. 4. Comparison of the Fourier and KCM heat-flux profiles along the line intersecting the center of two contiguous pores in holey film B at different temperatures.

V. CONCLUDING REMARKS

We present a multiscale hydrodynamic model designed to predict heat transport in complex geometries at small scales and low temperatures. The model equation is derived from the BTE. The equation coefficients, the bulk thermal conductivity, and the nonlocal length are intrinsic quantities (i.e., not dependent on geometry) and can be obtained from *ab initio* calculations. In contrast to previous models, where boundary effects are included through boundary scattering rates in a Matthiessen rule, here the system geometry is incorporated through the boundary conditions. The simplicity of the equations allows us to obtain numerical solutions in arbitrary geometries by using finite-element methods. This permits specific predictions that can be compared with experimental data.

To verify the model, we compare it with experimental data in stationary situations for silicon samples with two different geometries: compact and holey thin films. Agreement is found between model predictions and experimental data for both geometries in a wide range of sizes and temperatures. At sufficiently small sizes or low temperatures, however, the model systematically underestimates the data. Remarkably, we obtain a simple quantitative criterion specifying the region of predictability of the model: the smallest system dimension must be larger than twice the nonlocal length. This criterion corresponds to the case where there is no complete overlap of the nonlocal effects produced in different boundaries and is shown to be satisfied in the range of sizes and temperatures studied in both geometries. This result is consistent with previous work on heater lines on top of silicon, where non-Fourier behavior was observed [2,20]. There the hydrodynamic model was capable of reproducing the experimental results for line widths satisfying a similar criterion.

When all system sizes are larger than the phonon MFP, the effect of boundaries is restricted to a small region on the order of the MFP close to the boundaries. In the rest of the system, intrinsic collisions dominate and heat transport is diffusive. As the system size decreases, this region occupies a larger fraction of the whole system, so boundary effects become important: this is the hydrodynamic regime. For sizes smaller than twice the nonlocal length, the model predictions fail because the contribution of ballistic phonons to the thermal conductivity is important. Despite this, the model equation may still describe the experimental data by using effective parameters. For instance, in Refs. [2,20] heater-line experimental data could be described by use of a thermal conductivity greater than the calculated thermal conductivity. However, much

theoretical work is still needed to predict heat transport at very small scales.

Finally, some comments on the use of the term "hydrodynamic heat transport" are in order. In the literature, hydrodynamic heat transport is usually confined to the regime where normal collisions are dominant and boundary collisions start to play a role [27]. In this work, however, analogous to fluid flow, "hydrodynamic heat transport" refers to the situation where boundary effects are important so that the heat-flux profile becomes Poiseuille-like. This view applies to the usual definition, but it also includes the case when boundary effects result from resistive dominant collisions. The KCM thus describes the combined effect of normal and resistive collisions on the boundary layer through a single model equation. The agreement between the model and experimental data presented in this work opens the door to the use of the hydrodynamic equation instead of an effective Fourier model to interpret current heat-transport experimental data.

ACKNOWLEDGMENTS

We acknowledge the financial support of the Spanish Ministry of Economy and Competitiveness under Consolider nanoTHERM Grant No. CSD2010-00044, Grant No. TEC2015-67462-C2-2-R (MINECO/FEDER), and Grant No. TEC2015-67462-C2-1-R (MINECO/FEDER), and the support of the Department d'Universitats, Recerca i Societat de la Informació (DURSI) of the Generalitat de Catalunya under Grant No. 2017-SGR-1018. The research leading to these results was partially funded by the CERCA program of the Generalitat de Catalunya. M.C. acknowledges that the research leading to these results received funding from the La Caixa Foundation. T.M. acknowledges the support of the Spanish Ministry of Economy and Competitiveness under Grant No. MTM2017-82317-P.

APPENDIX: NUMERICAL SOLUTIONS OF THE HYDRODYNAMIC-HEAT-TRANSPORT EQUATION

This appendix describes the Galerkin-method implementation [32] to obtain numerical solutions of Eqs. (1) and (2) with boundary conditions (3) and (4). The first step is to obtain the weak form of Eq. (1) by multiplication by a linear test function $\hat{T}$ of the temperature and integration over the volume Ω:

$$\int_\Omega \hat{T}\left(c\frac{T}{dt}+\nabla\cdot\mathbf{q}\right)d\Omega=0. \tag{A1}$$

To obtain the weak form of the hydrodynamic-heat-transport equation (2), we define a tensor σ analogous to the stress tensor used for the compressible NSE:

$$\sigma=l^2\nabla\mathbf{q}+2\ell^2\nabla\cdot\mathbf{q}\mathbb{I}-\kappa T\mathbb{I}, \tag{A2}$$

where $\mathbb{I}$ is the identity matrix. Equation (2) then reads

$$\tau\frac{\partial\mathbf{q}}{\partial t}+\mathbf{q}=\nabla\cdot\sigma. \tag{A3}$$

Now we multiply this by a quadratic test function $\hat{\mathbf{q}}$ of the heat flux and integrate by parts over the volume:

$$\int_\Omega\hat{\mathbf{q}}\left(\mathbf{q}+\tau\frac{\partial\mathbf{q}}{\partial t}\right)d\Omega=\int_\Omega\nabla\cdot(\hat{\mathbf{q}}\cdot\sigma)d\Omega-\int_\Omega\nabla\hat{\mathbf{q}}:\sigma\,d\Omega. \tag{A4}$$

The first term on the right-hand side can be expressed as a surface integral with use of the divergence theorem:

$$\int_\Omega\hat{\mathbf{q}}\left(\mathbf{q}+\tau\frac{\partial\mathbf{q}}{\partial t}\right)d\Omega=\oint_\Gamma(\sigma\cdot\mathbf{n})\cdot\hat{\mathbf{q}}d\Gamma-\int_\Omega\nabla\hat{\mathbf{q}}:\sigma\,d\Omega, \tag{A5}$$

where Γ is the boundary surface and $\mathbf{n}$ is the boundary normal vector.

When approximating T and $\mathbf{q}$ by a linear combination of functions in Eqs. (A1) and (A5), we obtain an independent equation for each test function in the same function space. To obtain an approximate solution, the resulting linear system of equations is solved numerically to obtain the coefficients of the linear combinations. The surface integral in Eq. (A5) is used to impose the boundary conditions (3) and (4) through discontinuous Galerkin methods [33].

From Eq. (A5), we identify the Lagrange multiplier $\lambda=\sigma\cdot\mathbf{n}$. We want to impose different conditions for the different components of the heat flux. Hence, the surface integral of λ is included as a weak contribution by projecting λ only with the heat-flux boundary-normal-component test function:

$$\oint_\Gamma\lambda\cdot(\hat{\mathbf{q}}\cdot\mathbf{n})\mathbf{n}d\Gamma. \tag{A6}$$

Considering λ as a new variable that is also approximated in the boundary by a linear combination of functions, we are able to impose Eq. (4) with the following condition:

$$\oint_\Gamma\hat{\lambda}\cdot(\mathbf{q}\cdot\mathbf{n})\mathbf{n}d\Gamma=0. \tag{A7}$$

Notice now that the surface integral of λ projected by the tangential component of the heat-flux test function also appears in Eq. (A5). Hence, by including the weak contribution

$$-\oint_\Gamma\frac{l}{C}\hat{\mathbf{q}}_t\cdot\mathbf{q}_t d\Gamma, \tag{A8}$$

we are able to impose Eq. (3).

Finally, a weak contribution for stabilization is required (see Ref. [33] for details):

$$-\oint_{\Gamma} l^2 O[m](\hat{\mathbf{q}}\cdot\mathbf{n})(\mathbf{q}\cdot\mathbf{n})d\Gamma = 0, \tag{A9}$$

where $O[m]$ is a coefficient depending on the discretization-element surface-to-volume ratio.

In the compact and holey thin films, periodic heat-flux conditions are required to reproduce the whole geometry by simulating only a periodically repeated unit. The procedure is the same as that for imposing Eq. (4) but with averaging between boundaries the Lagrange multiplier and averaging all the components of $\mathbf{q}$ and $\hat{\mathbf{q}}$. Let us denote as 1 and 2 the boundaries in which the periodic condition is imposed. Then the average normal component of σ is

$$\lambda_{\mathrm{av}} = \frac{1}{2}(\lambda_1 + \lambda_2) = \frac{1}{2}(\mathbf{n}_1\cdot\sigma_1 + \mathbf{n}_2\cdot\sigma_2), \tag{A10}$$

where $\mathbf{n}_1$ and $\mathbf{n}_2$ are the boundary normal vectors ($\mathbf{n}_1 = -\mathbf{n}_2$). A temperature jump between boundary 1 and boundary 2 can be imposed by mapping the temperature appearing in σ_1 and σ_2 and imposing a difference ΔT. Half of the required weak contributions, including the stabilization contribution, are imposed in each boundary. For $i = 1, 2$,

$$\oint_{\Gamma_i} \lambda_{\mathrm{av}}\cdot\frac{1}{2}\hat{\mathbf{q}}_i d\Gamma_i + \oint_{\Gamma_i} \hat{\lambda}_i\cdot\frac{1}{2}(\mathbf{q}_1 - \mathbf{q}_2)d\Gamma_i - \oint_{\Gamma_i} l^2 O[m](\mathbf{q}_1 - \mathbf{q}_2)\cdot\hat{\mathbf{q}}_i d\Gamma_i. \tag{A11}$$

[1] ITRS, International Technology Roadmap for Semiconductors 2.0: Executive Report, International technology roadmap for semiconductors, 79 (2015).

[2] Amirkoushyar Ziabari, Pol Torres, Bjorn Vermeersch, Yi Xuan, Xavier Cartoixà, Alvar Torelló, Je-Hyeong Bahk, Yee Rui Koh, Maryam Parsa, Peide D. Ye, F. Xavier Alvarez, and Ali Shakouri, Full-field thermal imaging of quasiballistic crosstalk reduction in nanoscale devices, Nat. Commun. **9**, 255 (2018).

[3] Mark E. Siemens, Qing Li, Ronggui Yang, Keith A. Nelson, Erik H. Anderson, Margaret M. Murnane, and Henry C. Kapteyn, Quasi-ballistic thermal transport from nanoscale interfaces observed using ultrafast coherent soft X-ray beams, Nat. Mater. **9**, 26 (2010).

[4] Kathleen M. Hoogeboom-Pot, Jorge N. Hernandez-Charpak, Xiaokun Gu, Travis D. Frazer, Erik H. Anderson, Weilun Chao, Roger W. Falcone, Ronggui Yang, Margaret M. Murnane, Henry C. Kapteyn, and Damiano Nardi, Anew regime of nanoscale thermal transport: Collective diffusion increases dissipation efficiency, Proc. Natl. Acad. Sci. U. S. A. **112**, 4846 (2015).

[5] R. A. Guyer and J. A. Krumhansl, Solution of the linearized phonon Boltzmann equation, Phys. Rev. **148**, 766 (1966).

[6] Joseph Callaway, Model for lattice thermal conductivity at low temperatures, Phys. Rev. **113**, 1046 (1959).

[7] Yangyu Guo and Moran Wang, Phonon hydrodynamics for nanoscale heat transport at ordinary temperatures, Phys. Rev. B **97**, 035421 (2018).

[8] Vazrik Chiloyan, Lingping Zeng, Samuel Huberman, Alexei A. Maznev, Keith A. Nelson, and Gang Chen, Variational approach to solving the spectral Boltzmann transport equation in transient thermal grating for thin films, J. Appl. Phys. **120**, 025103 (2016).

[9] D. L. Nika, A. S. Askerov, and A. A. Balandin, Anomalous size dependence of the thermal conductivity of graphene ribbons, Nano Lett. **12**, 3238 (2012).

[10] David A. Broido, M. Malorny, G. Birner, Natalio Mingo, and D. A. Stewart, Intrinsic lattice thermal conductivity of semiconductors from first principles, Appl. Phys. Lett. **91**, 231922 (2007).

[11] Andrea Cepellotti and Nicola Marzari, Thermal Transport in Crystals as a Kinetic Theory of Relaxons, Phys. Rev. X **6**, 041013 (2016).

[12] Laurent Chaput, Direct Solution to the Linearized Phonon Boltzmann Equation, Phys. Rev. Lett. **110**, 265506 (2013).

[13] Wu Li, Natalio Mingo, L. Lindsay, David A. Broido, D. A. Stewart, and N. A. Katcho, Thermal conductivity of diamond nanowires from first principles, Phys. Rev. B **85**, 195436 (2012).

[14] Zhao Wang and Natalio Mingo, Diameter dependence of SiGe nanowire thermal conductivity, Appl. Phys. Lett. **97**, 101903 (2010).

[15] Zhiwei Ding, Jiawei Zhou, Bai Song, Vazrik Chiloyan, Mingda Li, Te Huan Liu, and Gang Chen, Phonon hydrodynamic heat conduction and Knudsen minimum in graphite, Nano Lett. **18**, 638 (2018).

[16] Antonio Sellitto, Vito Antonio Cimmelli, and David Jou, *Mesoscopic Theories of Heat Transport in Nanosystems*, Series SEMA SIMAI Springer Series Vol. 6 (Springer, International Publishing, Cham, 2016).

[17] C. de Tomas, A. Cantarero, A. F. Lopeandia, and F. X. Alvarez, From kinetic to collective behavior in thermal transport on semiconductors and semiconductor nanostructures, J. Appl. Phys. **115**, 164314 (2014).

[18] Moran Wang, Nuo Yang, and Zeng-Yuan Guo, Non-fourier heat conductions in nanomaterials, J. Appl. Phys. **110**, 064310 (2011).

[19] P. Torres, A. Torelló, J. Bafaluy, J. Camacho, X. Cartoixà, and F. X. Alvarez, First principles kinetic-collective thermal conductivity of semiconductors, Phys. Rev. B **95**, 165407 (2017).

[20] P. Torres, A. Ziabari, A. Torelló, J. Bafaluy, J. Camacho, X. Cartoixà, A. Shakouri, and F. X. Alvarez, Emergence of hydrodynamic heat transport in semiconductors at the nanoscale, Phys. Rev. Mater. **2**, 076001 (2018).

[21] Amr M. S. Mohammed, Yee Rui Koh, Bjorn Vermeersch, Hong Lu, Peter G. Burke, Arthur C. Gossard, and Ali Shakouri, Fractal lévy heat transport in nanoparticle embedded semiconductor alloys, Nano Lett. **15**, 4269 (2015).

[22] Bjorn Vermeersch, Amr M. S. Mohammed, Gilles Pernot, Yee Rui Koh, and Ali Shakouri, Superdiffusive heat conduction in semiconductor alloys. II. Truncated Lévy

formalism for experimental analysis, Phys. Rev. B **91**, 085203 (2015).

[23] Bjorn Vermeersch, Jesús Carrete, Natalio Mingo, and Ali Shakouri, Superdiffusive heat conduction in semiconductor alloys. I. Theoretical foundations, Phys. Rev. B - Condens. Matter Mater. Phys. **91**, 085202 (2015).

[24] P. Torres, F. X. Alvarez, and X. Cartoixa, Kinetic Collective Model: BTE-based hydrodynamic model for thermal transport, https://physta.github.io.

[25] F. X. Alvarez, D. Jou, and A. Sellitto, Phonon hydrodynamics and phonon-boundary scattering in nanosystems, J. Appl. Phys. **105**, 014317 (2009).

[26] M. Asheghi, M. N. Touzelbaev, K. E. Goodson, Y. K. Leung, and S. S. Wong, Temperature-dependent thermal conductivity of single-crystal silicon layers in SOI substrates, J. Heat Transfer **120**, 30 (1998).

[27] J. M. Ziman, *Electrons and Phonons: The Theory of Transport Phenomena in Solids* (Oxford University Press, Amen House, London, UK, 2001).

[28] M. Asheghi, K. Kurabayashi, R. Kasnavi, and K. E. Goodson, Thermal conduction in doped single-crystal silicon films, J. Appl. Phys. **91**, 5079 (2002).

[29] W. Liu and M. Asheghi, Phonon-boundary scattering in ultrathin single-crystal silicon layers, Appl. Phys. Lett. **84**, 3819 (2004).

[30] Martin Maldovan, Micro to nano scale thermal energy conduction in semiconductor thin films, J. Appl. Phys. **110**, 034308 (2011).

[31] David Song and Gang Chen, Thermal conductivity of periodic microporous silicon films, Appl. Phys. Lett. **84**, 687 (2004).

[32] Olek Zienkiewicz, Robert Taylor, and J. Z. Zhu, *The Finite Element Method: Its Basis and Fundamentals* (Butterworth-Heinemann, Oxford, 2013), 7th ed.

[33] O. C. Zienkiewicz, R. L. Taylor, S. J. Sherwin, and J. Peiró, On discontinuous Galerkin methods, Int. J. Numer. Methods. Eng. **58**, 1119 (2003).